



HAL
open science

Changes in effective stress during the 2003-2004 Ubaye seismic swarm, France

Guillaume Daniel, Elodie Prono, Francois Renard, François Thouvenot, S. Hainzl, David Marsan, Agnès Helmstetter, P. Traversa, Jean-Luc Got, Liliane Jenatton, et al.

► **To cite this version:**

Guillaume Daniel, Elodie Prono, Francois Renard, François Thouvenot, S. Hainzl, et al.. Changes in effective stress during the 2003-2004 Ubaye seismic swarm, France. *Journal of Geophysical Research : Solid Earth*, 2011, 116, pp.B01309. 10.1029/2010JB007551 . insu-00679798

HAL Id: insu-00679798

<https://insu.hal.science/insu-00679798>

Submitted on 2 Mar 2021

HAL is a multi-disciplinary open access archive for the deposit and dissemination of scientific research documents, whether they are published or not. The documents may come from teaching and research institutions in France or abroad, or from public or private research centers.

L'archive ouverte pluridisciplinaire **HAL**, est destinée au dépôt et à la diffusion de documents scientifiques de niveau recherche, publiés ou non, émanant des établissements d'enseignement et de recherche français ou étrangers, des laboratoires publics ou privés.

Changes in effective stress during the 2003–2004 Ubaye seismic swarm, France

G. Daniel,¹ E. Prono,² F. Renard,^{3,4} F. Thouvenot,³ S. Hainzl,⁵ D. Marsan,²
A. Helmstetter,³ P. Traversa,³ J. L. Got,² L. Jenatton,³ and R. Guiguet³

Received 15 March 2010; revised 8 October 2010; accepted 19 October 2010; published 29 January 2011.

[1] We study changes in effective stress (normal stress minus pore pressure) that occurred in the French Alps during the 2003–2004 Ubaye earthquake swarm. Two complementary data sets are used. First, a set of 974 relocated events allows us to finely characterize the shape of the seismogenic area and the spatial migration of seismicity during the crisis. Relocations are performed by a double-difference algorithm. We compute differences in travel times at stations both from absolute picking times and from cross-correlation delays of multiplets. The resulting catalog reveals a swarm alignment along a single planar structure striking N130°E and dipping 80°W. This relocated activity displays migration properties consistent with a triggering by a diffusive fluid overpressure front. This observation argues in favor of a deep-seated fluid circulation responsible for a significant part of the seismic activity in Ubaye. Second, we analyze time series of earthquake detections at a single seismological station located just above the swarm. This time series forms a dense chronicle of +16,000 events. We use it to estimate the history of effective stress changes during this sequence. For this purpose we model the rate of events by a stochastic epidemic-type aftershock sequence model with a nonstationary background seismic rate $\lambda_0(t)$. This background rate is estimated in discrete time windows. Window lengths are determined optimally according to a new change-point method on the basis of the interevent times distribution. We propose that background events are triggered directly by a transient fluid circulation at depth. Then, using rate-and-state constitutive friction laws, we estimate changes in effective stress for the observed rate of background events. We assume that changes in effective stress occurred under constant shear stressing rate conditions. We finally obtain a maximum change in effective stress close to -8 MPa, which corresponds to a maximum fluid overpressure of about 8 MPa under constant normal stress conditions. This estimate is in good agreement with values obtained from numerical modeling of fluid flow at depth, or with direct measurements reported from fluid injection experiments.

Citation: Daniel, G., et al. (2011), Changes in effective stress during the 2003–2004 Ubaye seismic swarm, France, *J. Geophys. Res.*, 116, B01309, doi:10.1029/2010JB007551.

1. Introduction

[2] Seismic swarms are dense and intensive episodes of microseismic activity. Generally, they do not consist in a simple succession of many larger shocks and their after-

shocks. They rather exhibit a complex behavior, compared to typical seismic crisis, initiating with an increasing number of small events and ending after a variable term. The study of these phenomena is thus very challenging, as they question the very detailed behavior of seismicity. Seismic swarms also reflect transient changes of in situ physical properties in the upper crust. Consequently, the analysis of swarm episodes is of importance, as it may potentially bear crucial information on the general earthquake preparation process at a human time scale.

[3] This study focuses on the Ubaye valley area (Alpes-de-Haute-Provence, France; see Figure 1), which is the most seismically active region in the French western Alps [Thouvenot and Fréchet, 2006]. Seismic activity in this area is characterized both by moderate earthquakes (e.g.,

¹UMR 6249 Chrono-environnement, CNRS-Université de Franche-Comté, Besançon, France.

²LGIT, Université de Savoie, CNRS, Observatoire de Grenoble, Le Bourget du Lac, France.

³LGCA, Université Joseph Fourier-Grenoble I, CNRS, Observatoire de Grenoble, Grenoble, France.

⁴Also at Physics of Geological Processes, University of Oslo, Oslo, Norway.

⁵Institute of Geosciences, University of Potsdam, Potsdam, Germany.

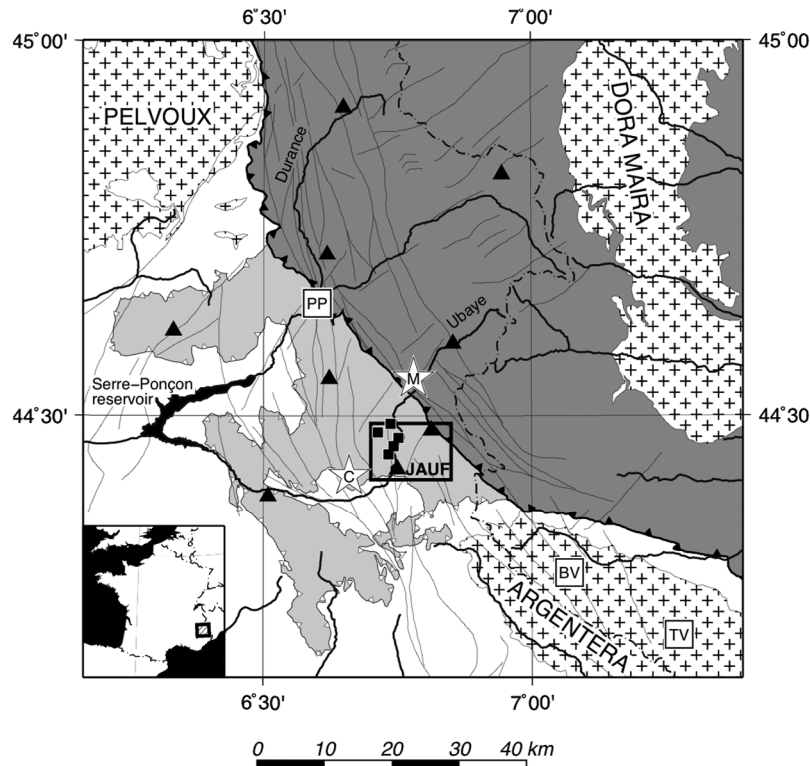


Figure 1. Map of the southwestern Alps with main geological features. Crossed areas stand for the Pelvoux, Argentera, and Dora Maira crystalline massifs. The lightly shaded area is the Embrunnais-Ubaye nappes. The dark gray area is the Peninnic domain. Fault traces are after *Sue* [1998]. Stars correspond to macroseismic (M) and computed (C) epicenters of the 1959 M 5.5 Saint Paul-sur-Ubaye damaging earthquake. Triangles are permanent seismological stations from the Sismalp network, and squares stand for temporary seismological stations deployed in the area from September 2003. Hot springs are also indicated: BV, Bagni di Vinadio; PP, Plan de Phasy; and TV, Terme di Valdieri. The dash-dotted line is the French-Italian border. The study area is delimited by the box in the center of the map. Modified from *Jenatton et al.* [2007].

the historical M 5.5 Saint Paul-sur-Ubaye earthquake in 1959) and episodic swarms. Using a temporary seismological network, *Fréchet and Pavoni* [1979] conducted the first study of a swarm in Ubaye. Subsequently, *Guyoton et al.* [1990] described another swarm episode in 1989, soon after the installation of the permanent seismological network Sismalp (<http://sismalp.obs.ujf-grenoble.fr/>). They located it 5 km NE of Saint Paul. In the present study, we analyze the most recent swarm episode in this area, which started in January 2003 close to La Condamine-Châtelard (see Figure 1). This swarm consisted in a period of continuous seismic activity that lasted about 2 years. This sequence thus represents a new opportunity to improve our knowledge on the mechanics of swarm generation, and to study active faults in the Ubaye area.

[4] In the literature, swarm occurrence is commonly related to the circulation of deep-seated fluids along, or in the vicinity of earthquake faults. Aseismic creep can also constitute an alternative trigger mechanism [*Lohman and McGuire*, 2007]. The close association between fluids and swarm relies either on direct observations of surface fluid flow accompanying the seismic activity (e.g., during the 1965–1967 Matsushiro swarm, Japan [see *Tsuneishi and Nakamura*, 1970]), or on the close association of swarm

episodes with areas of important gas outflow (e.g., the western Eger rift, Bohemia, Czech Republic [*Weinlich et al.*, 1999; *Hainzl and Ogata*, 2005; *Bräuer et al.*, 2009] and the central Apennines, Italy [*Chiodini et al.*, 2000]). Frequently, swarms occur in regions of geothermal or volcanic activity (e.g., swarms in the Long Valley Caldera, California [*Savage and Cockerham*, 1984; *Hill and Prejean*, 2005]; at the Yellowstone volcanic field, western United States [*Farrell et al.*, 2009]; or east of the Izu Peninsula, Japan [*Ukawa and Tsukahara*, 1996]). These peculiar settings suggest that stress perturbations associated with fluid overpressure at depth is a plausible mechanism for the driving of seismic swarms [e.g., *Yamashita*, 1999; *Hainzl and Ogata*, 2005].

[5] During the Ubaye swarm, no fluid outflow was observed at the surface. However, the location of several hot springs located few tens of kilometers northward and southward from the study area reveals that current fluid circulations take place within the bedrock (Figure 1). According to these regional settings and to previous studies of swarms worldwide, we show here that a triggering of the Ubaye swarm by fluid overpressure is a very likely hypothesis. This hypothesis provides a coherent framework to explain the seismological observations. In section 2, we present the data set elaborated for the Ubaye seismic swarm. We describe the spatiotemporal

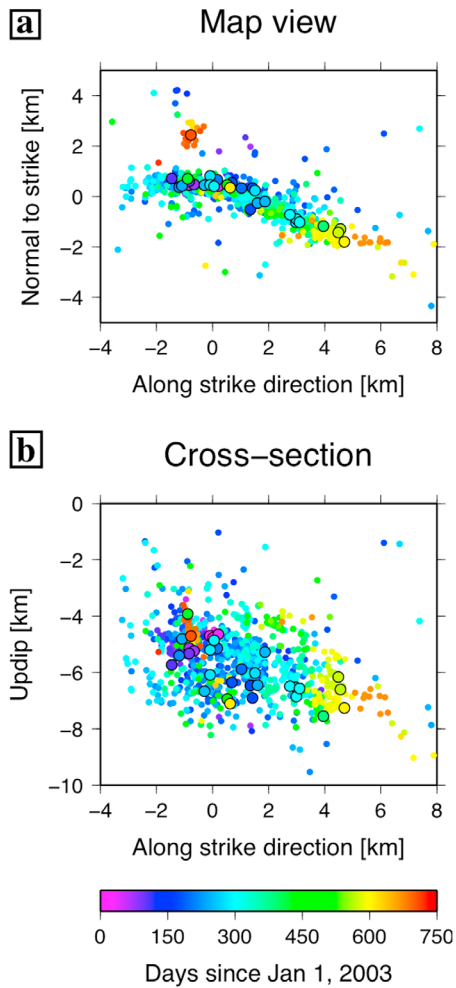


Figure 2. Map of the Ubaye 2003–2004 seismic swarm. A relocation of 974 seismic events is shown (a) in map view and (b) in cross section. Coordinates are projected on a planar orientation striking $N130^{\circ}E$ and dipping $80^{\circ}W$. Origins of coordinate axes correspond to the surface projection of the swarm centroid (with geographical coordinates $44^{\circ}27.2'N$, $6^{\circ}45'E$). Depth is expressed relatively to the sea level. Small dots stand for events with magnitude <2 , and large dots represent earthquakes with magnitude ≥ 2 . The colorscale highlights the date of each earthquake from January 2003 (magenta) to December 2004 (red).

evolution of the relocated data set in section 3, and present the characteristics of a diffusive migration pattern. In section 4 we model the rate of events and introduce a new objective statistical procedure to estimate the nonstationary background forcing rate in discrete time windows. In section 5 we estimate the amplitude of the effective stress changes leading to the observed earthquake rate, deduced from the rate-and-state constitutive laws [Dieterich, 1994]. We finally discuss our results in section 6.

2. Data

[6] This study relies on the analysis of two complementary seismological data sets. The first one is a relocated

catalog of microearthquakes, with magnitudes ranging between -0.3 and 2.7 . This data set was originally located by the Sismalp seismological network [Thouvenot *et al.*, 1990]. The second data set consists in a report of (hand-picked) event detections at JAUF, the closest seismological station (Figure 1). This station was located right above the earthquake swarm and allowed the detection of a large number of small events. This report constitutes a chronicle of 16,147 detections with M_L estimates ranging from -1.3 to 2.7 [Jenatton *et al.*, 2007].

2.1. Relocated Catalog

[7] Less than 10% of the 16,147 microearthquakes that occurred in Ubaye during years 2003 and 2004 were detected by a sufficient number of stations to be located. We have reprocessed the catalog of earthquake relocations originally presented in the work of Jenatton *et al.* [2007]. For this purpose, we have included phase picks at 5 supplementary stations (deployed in the area from September 2003 to December 2004) and improved its accuracy by using travel times estimated from the cross correlation of similar events (multiplets). All manual phase picks and cross-correlation delays were merged in a double-difference algorithm using the HYPODD software [Waldhauser and Ellsworth, 2000]. The main advantage of this relocation technique is that it allows the whole set of events to be located in a single operation. It also preserves the high accuracy of relative relocations within the multiplet.

[8] We obtain one single large multiplet of 799 events with a mean coherence greater than or equal to 90% on at least 3 stations. High-precision travel time delay measurements were performed by pair-wise cross correlation of the first 1.28 s of seismic waveforms in the spectral domain.

[9] The computation of relocation uncertainties by a Monte Carlo analysis led to an average location error of 100 m. The relocated catalog thus consists in 1058 events that occurred between years 1989 and 2004. Among these, 974 earthquakes occurred during the crisis in 2003–2004 and are displayed in Figure 2. We present a map view (Figure 2a) and a cross section (Figure 2b) of the swarm, with events coordinates projected along a plane trend of azimuth $N130^{\circ}E$ and dip $80^{\circ}W$.

2.2. Detection Time Series at Station JAUF

[10] The permanent seismological station JAUF recorded 16,147 events that could be hand-picked. Differences in P and S waves arrival times were analyzed to select only events occurring within the swarm area. Unfortunately, most of them could not be located as they triggered too few or no other stations. Event magnitudes were estimated from peak amplitudes of seismograms and distances, according to a calibration based on located events of the sequence [Jenatton *et al.*, 2007]. Magnitudes of this time series span from -1.3 up to 2.7 , leading to a total energy release equivalent to that of a magnitude 4 event. These authors also showed that magnitudes are consistent with a Gutenberg-Richter law [Gutenberg and Richter, 1956] with a b value of 1.2 ± 0.03 . The time series contains 3546 events with magnitude greater than the completeness threshold $M_L = 0.2$. This threshold has been determined by visual inspection on the basis of the validity of Gutenberg-Richter law for higher magnitudes. We here use origin times at JAUF to

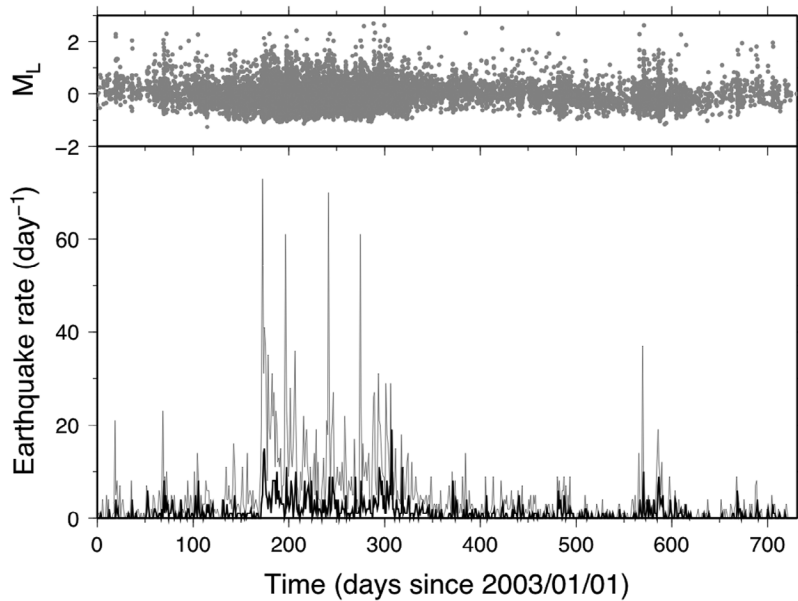


Figure 3. (top) Time series and magnitudes of the 16,147 events recorded at station JAUF between 1 January 2003 (day 0) and 31 December 2004 (day 730). (bottom) Rate of $M_L \geq 0.2$ earthquakes detected at station JAUF (gray curve) and of $M_L \geq 1$ earthquakes relocated in this study (black curve; see also Figure 2).

calculate the swarm seismicity rate (Figure 3, gray line). For the sake of comparison, and in order to verify that both data sets present a similar temporal evolution, we displayed the rate of the 974 relocated earthquakes in Figure 3 (black curve).

3. Spatial Evolution of the Swarm

[11] This section focuses on two main features of the relocated catalog. First, it reveals a precise image of the fault zone geometry (section 3.1) and second, it suggests a peculiar temporal evolution of the seismic activity along this structure (section 3.2).

3.1. Geometry of the Seismogenic Structure

[12] In map view (see Figure 2a), the Ubaye swarm appears as an elongated narrow cloud of microearthquakes. The seismicity is mainly located within a narrow 8 km long and 1 km wide band. At depth, all events are located on a quasi-vertical structure. This, however, does not guarantee that the seismic activity occurred on a single fault. Such a cloud may as well be defined, for example, by events distributed along a dense network of numerous short faults with different orientations. We now aim at determining the fault zone structure associated with this swarm. We assume that microearthquakes are not randomly distributed within a volume but rather occur along planar faults/fractures. We then search for the preferential plane orientations, by a simple geometrical analysis of hypocenters spatial distribution.

[13] We use the three point method [Fehler *et al.*, 1987] to detect preferential planar alignments of hypocenters. This method relies on the distribution of plane orientations (strike, dip) obtained for each possible set of 3 events in the relocated catalog (i.e., among 974 events). As the orientation of planes defined by close events will have larger

uncertainties because of locations errors, we restricted our analysis to events separated by at least 100 m. We also used a maximum separation distance of 10 km in order to remove events located far from the main swarm cluster. We remove the influence of the cluster elongated shape by normalizing the distribution of plane orientation with respect to 100 random location sets within a volume of comparable dimensions. We consider as significant every orientation occurring more than 3.62 standard deviations above the corresponding level obtained with the random data sets. This corresponds to a ratio of 1 chance in 10,000 that this preferential alignment be indicated by random variations around the mean number of similar orientations in the random data set [Fehler *et al.*, 1987]. The preferred plane then corresponds to the most frequent orientation above this threshold. This method also allows linking each seismic event with its preferred plane orientation, interpreted as the fracture plane on which this event most likely fell. For this purpose, we count how many times each event contributes to a set of 3 events aligned along a particular orientation. Events with the largest number of counts are those that occur along this particular plane.

[14] Orientations of preferential planes are presented in Figure 4. Polar histograms display the number of relocated earthquakes associated with each strike (see Figure 4a) and dip (see Figure 4b) orientation. They show a clear prominence for planes striking $N130^\circ E \pm 5^\circ$ and dipping $80^\circ \pm 5^\circ$ to the west, according to the convention used in the work of Aki and Richards [2002]. This range of orientations is in good agreement with the general trend of relocated seismicity, and is also close to the $N145^\circ E$ direction obtained by Jenatton *et al.* [2007] from the set of original locations. Interestingly, we find no preferential orientation striking perpendicular to the cloud elongation direction, dismissing any possible interplay of conjugate faults during this episode.

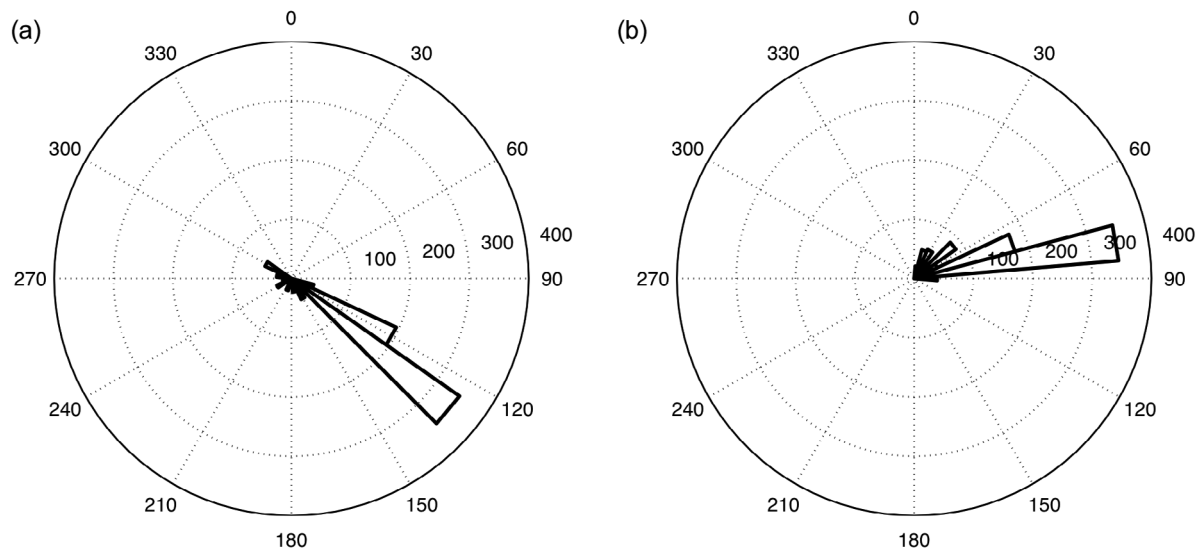


Figure 4. Distributions of (a) strike and (b) dip angles for planes associated with seismic events of the relocated catalog. Plane orientations were estimated for each possible set of three earthquakes using the method of *Fehler et al.* [1987]. Sector length indicates the number of earthquakes associated with each plane orientation. In Figure 4a the sector direction indicates the azimuth of planes, with 0° and 90° standing for the north and east directions, respectively. Bins are 10° wide. A clear preeminence exists for events occurring along planes striking N130°E and dipping 80° W.

We also notice that no temporal pattern is discernible in the evolution of the preferred orientation. Rather, the whole range of orientations represented in Figure 4 is associated with events from the initiation to the ending of the swarm episode. All these observations clearly argue in favor of a single seismogenic discontinuity at depth striking NW-SE and dipping 80° W.

3.2. Migration of the Swarm Activity

[15] The most striking feature of the Ubaye crisis is certainly its temporal evolution. This is highlighted in Figure 2 by a color-scaling of hypocenters depending on their date of occurrence. Relocated events exhibit a quasi-unilateral migration of microearthquakes from the NW to the SE, within a band located between 3 and 8 km at depth.

[16] We here discuss the diffusive character of the Ubaye swarm migration. For this purpose, we measure the progressive spreading of the main swarm cluster during the sequence. For each time t , we compute the average distance R between all events that occurred at time $t_i < t$ and the first earthquake of the sequence (Figure 5). Several previous studies have already documented the evolution of this distance R for earthquake sequences [Noir *et al.*, 1997; Marsan *et al.*, 1999, 2000; Helmstetter *et al.*, 2003b; Huc and Main, 2003]. For various global or regional earthquake catalogs, these authors found that R increases slowly with time, according to $R(t) \propto t^H$ with H close to 0.1 or 0.2. Helmstetter *et al.* [2003b] also noticed that this H value may vary from one individual sequence to another, and depends on the methods used to measure R . Such a relationship reveals that if a stress diffusion mechanism takes place within Earth's crust, it occurs slowly, and may be very weak [Marsan *et al.*, 2000; Huc and Main, 2003].

[17] Inspection of Figure 5 reveals that the seismic activity in Ubaye started to spread about 30 days after the swarm

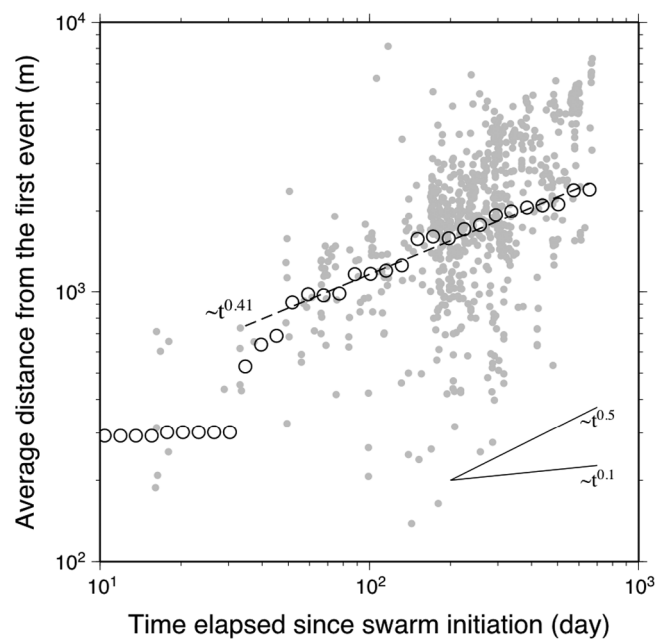


Figure 5. Characteristic size R of the main swarm cluster as a function of time. For a given time t , R is measured as the average distance between all swarm events that occurred at time $t_i < t$ and the first earthquake of the sequence. After ~ 30 days of relative stability, this average distance increases as $R \sim t^H$ with $H = 0.41 \pm 0.06$. For the sake of comparison we have represented in the lower right corner slopes that should be expected for a normal diffusive process ($H = 0.5$) and for a typical subdiffusive process expected during aftershock sequences ($H = 0.1$). Information on the spreading of the data is given by the gray circles, which indicate the distance between every relocated earthquake and the first one of the sequence.

initiation. The average distance R increases up to the end of 2004, mainly along the preferential plane orientation (see also Figure 2). Interestingly, the spreading of the Ubaye sequence exhibits a quasi-diffusive character, characterized by a diffusion exponent value $H = 0.41 \pm 0.06$. Thus, not only did this swarm migrate very clearly, but also this migration took place according to a process closer to a normal diffusion (i.e., with $H = 0.5$) than to the subdiffusive process expected for typical earthquake sequences.

[18] Normal diffusion processes characterize particle motions in physical systems close to equilibrium (e.g., L. Vlahos et al., Normal and anomalous diffusion: A tutorial, 2008, available at <http://arxiv.org/abs/0805.0419>). Within Earth's crust, such behavior may either be related to a viscous relaxation mechanism, or to a pore pressure balancing mechanism induced by fluid flow in a relatively homogeneous medium. In Ubaye, as the depth of relocated hypocenters lies within the upper, elastic, brittle part of the crust, we rather support the latter mechanism; i.e., fluids. We argue that a deep increase in pore pressure by fluid flow is the most likely mechanism, and could unclamp favorably oriented faults/fractures by decreasing the effective normal stress. In other words, we claim that seismicity in Ubaye is the result of a nonstationary forcing by fluids, a well-known likely mechanism for the generation of earthquakes [e.g., Nur and Booker, 1972].

[19] For several years hydraulic fracturing studies have been focusing on the relationship between such temporal spreading of the microseismicity and physical properties of the fractured medium; e.g., permeability [see, e.g., Shapiro et al., 1997, 2006b]. Although their approach appears very attractive to characterize the fracturing process taking place during the swarm, these physical models require boundary conditions, or experimental settings, quite unlikely for natural seismic swarms. For instance, a constant fluid injection rate may not be adequate for the Ubaye swarm, in reference with the size of the seismogenic volume and the long duration (2 years) of this episode. Nonetheless, the planar shape of the hypocenters cloud reveals that a fault zone with a higher permeability than the surrounding host rock was preexisting in the basement. When fluids invaded the medium during the swarm episode, this zone thus provided a natural channel for fluid circulation, and consequently, for earthquake occurrence. Recently, Shapiro and Dinske [2009] proposed a generalized model for microearthquakes migration that involves a nonlinear diffusion of fluids. According to their results, $H \neq 0.5$ may either follow from a pressure-dependent diffusivity parameter, or from a time varying fluid injection rate. These two mechanisms may have likely controlled the migration process observed in Ubaye.

4. Nonstationary Forcing of Seismicity by Fluids

[20] The driving of seismic swarms by fluids has been reported as a likely mechanism in numerous studies [e.g., Hill, 1977; Yamashita, 1999; Horálek and Fischer, 2008], although surface evidences of fluid flow are scarce [e.g., Tsuneishi and Nakamura, 1970]. Indeed in Ubaye no fluid outflow was observed during the sequence [Jenatton et al., 2007]. In the following, we hypothesize that a transient fluid circulation at depth led to a significant part of the swarm activity, the remaining part resulting from self-sustained

cascades of aftershocks [Hainzl and Ogata, 2005]. We have developed a new methodology in order to retrieve the rate of microearthquakes induced by a nonstationary background forcing in discrete time windows. We later associate this forcing with effective stress changes at depth. The procedure that we describe in the following aims at modeling the seismicity rate recorded at station JAUF as a stochastic process.

[21] The earthquake rate detected at JAUF (Figure 3) cannot be consistent with a typical main shock-aftershock sequence. In Ubaye, we could not model satisfactorily the sequence as a succession of aftershock sequences obeying the Omori law superimposed on a Poissonian background rate. Such a behavior would lead to a temporal seismic response similar to that modeled with an epidemic-type aftershock sequence (ETAS) model with a constant background seismicity term [Kagan and Knopoff, 1987; Ogata, 1988]. Conversely, suitable modeling of this sequence requires the involvement of a nonstationary background rate. Consequently, we model the earthquake time series in Ubaye by a time-dependent Poisson process. The probability to observe k seismic events during a time interval dt is given by

$$P(k|\Lambda) = e^{-\Lambda} \frac{\Lambda^k}{k!} \quad (1)$$

where

$$\Lambda = \int_{t-dt}^t \lambda(s) ds$$

The rate $\lambda(t)$ consists in the superposition of two distinct contributions: a nonstationary background term $\lambda_0(t)$ and an epidemic term $\lambda_e(t)$. This last term explicitly stands for the probability that each event of the sequence generates its own secondary aftershocks [Kagan and Knopoff, 1987; Ogata, 1988]:

$$\lambda(t) = \lambda_0(t) + \lambda_e(t) \quad (2)$$

with

$$\lambda_e(t) = \sum_{t_i < t} \frac{Ae^{\alpha(M_i - M_c)}}{(t - t_i + c)^p} \quad (3)$$

where t_i and M_i are the occurrence time and magnitude, respectively, of an earthquake i , whose magnitude is greater than, or equal to the magnitude of completeness M_c . A , α , c and p are epidemic parameters. This formulation has been used in previous studies to model seismicity rates and to retrieve the evolution of the nonstationary rate. Related studies by Hainzl and Ogata [2005] applied such modeling to the Vogtland-West Bohemia swarm, and Matsu'ura and Karakama [2005] to the Matsushiro swarm, Japan. Both studies improved significantly the modeling of seismicity rates with respect to an ETAS model with a constant background term $\lambda_0(t)$. In addition, Hainzl and Kraft [2006] related this nonstationary forcing $\lambda_0(t)$ to changes in pore pressure P according to

$$\lambda_0(t) = \lambda_{00} + K \frac{\partial P}{\partial t} \quad (4)$$

where λ_{00} is a constant background rate and K is a proportionality constant. This link was recently confirmed by *Llenos et al.* [2009], who showed that during swarm episodes, aseismic forcing (e.g., fluids or creep) influences preferentially the background activity rate rather than other epidemic parameters of the ETAS model.

[22] Model estimation is here performed in two steps. First, we determine an optimal set of discrete time windows and estimate their respective background rate $\lambda_0(t)$ for each time window on the basis of the distribution of earthquake interevent times. Second, we obtain the 4 epidemic parameters (A , α , c and p) that best explain the observed seismicity rate, using a maximum likelihood procedure.

4.1. Discretization of $\lambda_0(t)$

[23] Objective discretization of the function $\lambda_0(t)$ is an important concern. Indeed, there exists a tradeoff between a choice of long time windows (that preserve the epidemic character of the model but prevent to retrieve rapid changes of the forcing rate) and a choice of short time windows that tend to annihilate the epidemic contribution $\lambda_e(t)$. In the first situation, the model converges toward the original ETAS formulation [*Ogata*, 1988] as the length of time windows tends toward the length of the sequence. In the last situation, the model converges toward $\lambda(t) = \lambda_0(t)$ as the length of time windows tends toward 0. In both cases, we may miss crucial information concerning the interplay between a time-dependent external forcing $\lambda_0(t)$ and the self-triggering $\lambda_e(t)$ of the seismic activity.

[24] To overcome this difficulty, we here propose an objective procedure that optimizes the discretization of the time axis into separate intervals for the estimation of $\lambda_0(t)$. We aim at finding successive nonoverlapping time windows during which we consider the background external forcing $\lambda_0(t)$ as constant. The estimation of $\lambda_0(t)$ for each time window is based on the method of *Hainzl et al.* [2006] that builds upon the fact that the probability density function of interevent times can be expressed as

$$f(\delta t) = C \cdot e^{-a \cdot \delta t} \cdot (\delta t)^{-b} \quad (5)$$

with

$$C = \frac{a^{1-b}}{\Gamma(1-b)} \quad (6)$$

where δt are the interevent times, C is a normalization constant and Γ is the gamma function. *Hainzl et al.* [2006] showed that a and b can be estimated by

$$a = \frac{\overline{\delta t}}{\sigma_{\delta t}^2} \quad (7)$$

$$b = 1 - (\overline{\delta t} \cdot a) = 1 - \frac{\overline{\delta t}^2}{\sigma_{\delta t}^2} \quad (8)$$

We note that this approach relies on the hypothesis of independent interevent times, and that taking into account their interdependence may affect our results. Following these authors, we thus estimate the background rate as $\lambda_0(t) = a$. To evaluate the quality of the model $f(\tau)$, we divide the δt axis

into N bins $]0, \delta t_1],] \delta t_1, \delta t_2], \dots$ such that $\{\delta t_1, \delta t_2, \dots, \delta t_N\}$ are the observed interevent times ranked in ascending order. For a given bin $[\delta t_{i-1}, \delta t_i]$ we observe exactly one occurrence (δt_i) of the interevent times, while the model predicts

$$\mu_i = N \int_{\delta t_{i-1}}^{\delta t_i} d\delta t \cdot f(\delta t) \quad (9)$$

occurrences, on average. We thus define the likelihood $\ell = \prod_{i=1}^N e^{-\mu_i} \cdot \mu_i$ of the model, or equivalently

$$L = -\log(\ell) = \sum_{i=1}^N \mu_i - \ln(\mu_i) \quad (10)$$

Following the gamma law of *Hainzl et al.* [2006], equations (9) and (10) can be written as

$$\mu_i = N \cdot P(1-b, a \cdot \delta t_i) - N \cdot P(1-b, a \cdot \delta t_{i-1}) \quad (11)$$

$$L = -\log(\ell) = N \cdot P(1-b, a \cdot \delta t_N) - \sum_{i=1}^N \ln(\mu_i) \quad (12)$$

where P is the lower incomplete gamma function.

[25] In order to optimize the selection of time windows during which $\lambda_0(t)$ is modeled as constant, we use an objective change-point analysis. The rationale of the method is the following: let us consider a time period with N interevent times $\{\delta t_1, \delta t_2, \dots, \delta t_N\}$. We want to know if this time period is better characterized by a change in λ_0 at a time t such that there are N_1 interevent times for the time series prior to t and N_2 after t ($N = N_1 + N_2$). We thus compare the two hypotheses:

[26] 1. That $\lambda_0(t)$ does not vary significantly between these two windows, hence a single model $f(\delta t)$ can well describe the interevent time distribution for the time period;

[27] 2. That $\lambda_0(t)$ varies significantly between these two windows, and we need to define two distinct densities f_1 and f_2 , one for each window.

[28] In the first case, the log likelihood is L_1 as obtained from equation (12). In the second case, we compute L_2 from equations (9) and (12), but with

$$f(\delta t) = \frac{N_1}{N_1 + N_2} f_1(\delta t) + \frac{N_2}{N_1 + N_2} f_2(\delta t) \quad (13)$$

where f_1 and f_2 are parameterized independently for each window.

[29] We search for the best time t (i.e., the change point) by minimizing L_2 . This change point is then kept if L_2 is significantly lower than L_1 . An objective procedure is to use the Bayesian information criterion [*Davison*, 2003]:

$$\text{BIC} = 2L + n \ln(N) \quad (14)$$

where n is the number of free parameters in the model ($n_1 = 2$ in the first hypothesis of only one density, $n_2 = 5$ in the second hypothesis of two densities and a change point). We keep the change point if $\Delta \text{BIC} = 2 \cdot (L_2 - L_1) + (n_2 - n_1) \cdot \ln(N)$ is negative, hence $L_2 - L_1 < -3/2 \cdot \ln(N)$.

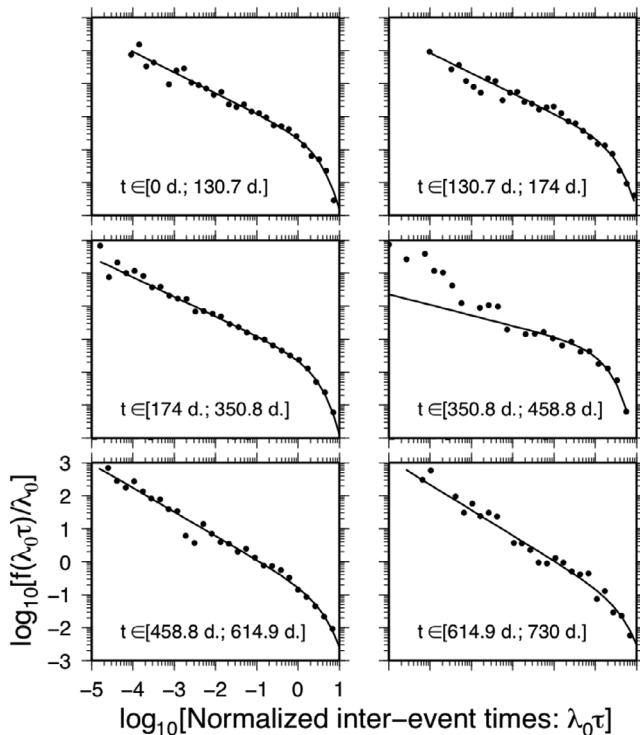


Figure 6. Adjustment of interevent times distributions (dots) by a Gamma distribution (curve) according to a maximum likelihood method. Each subplot corresponds to the interevent times distribution for a single time window with a constant background rate $\lambda_0(t)$. Time windows are defined by a change-point analysis on the basis of significant changes in successive interevent time distributions (see section 4.1).

Table 1. Limits of Optimal Time Windows and Amplitude of the Background Rate^a

Window Starting Time (days)	Window Ending Time (days)	$\lambda_0(t)$ (events/d)		
		Hainzl <i>et al.</i> 's [2006] Method	Alternative 1: Joint Inversion	Alternative 2: Background Reconstruction Method
0	130.7	1.06	0.92	0.66
130.7	174	2.52	3.04	2.93
174	350.8	4.99	3.79	2.84
350.8	458.8	1.78	0.76	0.35
458.8	614.9	0.65	0.41	0.21
614.9	730	0.24	0.27	0.03

^aHere we present background rate estimates obtained from three different algorithms. Best adjustments are obtained using Hainzl *et al.*'s [2006] method. Two alternative techniques were tested. Alternative 1 inverts jointly ETAS epidemic parameters and background values. Alternative 2 reconstructs the background rate from the difference between the observed rate of event and the rate of triggered events (obtained from the ETAS triggering kernel and A , α , c , and p estimates). The differences between the background estimates for the techniques of alternatives 1 and 2 may partly be due to the smoothing used for the background reconstruction technique (alternative 2) and to the use of different sets of ETAS parameters A , α , c , and p . See section 4.2.

[30] This procedure starts with the entire window and is iterated until no further change point is required. For the Ubaye swarm, we obtain a set of 6 discrete time windows for $\lambda_0(t)$ corresponding to the interval between two successive change points. Figure 6 displays the fit of empirical interevent times distributions by gamma distributions from equation (5). These diagrams show a good agreement between all interevent times and the gamma law. By estimating $\lambda_0(t)$ for each time interval associated with time windows defined according to this change point method, we ultimately provide the stair-step estimate of $\lambda_0(t)$ (see Figure 7, dashed line, and Table 1).

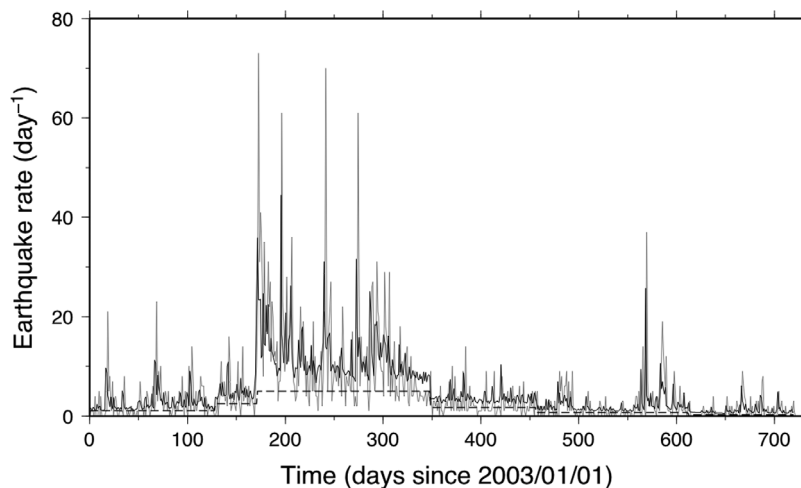


Figure 7. Comparison of the Ubaye seismic activity detected at station JAUF (gray curve) with the best nonstationary ETAS model (black curve); see equations (2) and (3). Best epidemic parameter estimates are $A = 0.0199$, $\alpha = 1.246$, $c = 1.35 \times 10^{-4}$ d and $p = 1.065$. The stair-step dashed line stands for the nonstationary background contribution $\lambda_0(t)$ to the seismicity rate. See Table 1 for a report on the amplitude of $\lambda_0(t)$ for each time window. This stair-step shape arises from the determination of optimal time windows with a constant background rate $\lambda_0(t)$, as determined by the change-point method explained in section 4.1. This method is based on interevent time adjustments presented in Figure 6.

4.2. Epidemic Parameters Estimate

[31] We estimate the best set of epidemic parameters $\hat{\theta} = \{A, \alpha, c, p\}$ by a maximum likelihood procedure. We define it as the one that maximizes the following log likelihood function:

$$L'(\theta) = \sum_k \ln \lambda(t_k; \lambda_0; \theta) - \int_0^T \lambda(t; \lambda_0; \theta) dt \quad (15)$$

where T is the duration of the catalog, and t_k are earthquake occurrence times. We suppose parameters A , α , c and p to be constant; i.e., we make the hypothesis that the self-triggering process remains the same during the whole swarm sequence. Considering the seismicity rate model given in equations (2) and (3), we note that for any θ , the log likelihood value will depend strongly on the shape of $\lambda_0(t)$. As our strategy for the estimation of θ relies on an independent estimate of $\lambda_0(t)$, this procedure guarantees a robust estimation of $\hat{\theta}$.

[32] Again, we use the BIC criterion (equation (14)) with $n = 4$ (number of epidemic parameters), $L = L'$ and $N = 3546$ to check that the ETAS model with a nonstationary rate $\lambda_0(t)$ significantly improves the modeling, with respect to the formulation involving only a stationary background seismicity rate. The nonstationary parameterization leads to a BIC value of $-10,304$, which is smaller than the value of -9880 obtained for the stationary background model. This decrease of the BIC criterion thus ensures that the nonstationary model provides a better fit to the data, while preserving a reasonable level of model complexity.

[33] Best epidemic parameters correspond to values of $A = 0.0199 \pm 0.0006$, $\alpha = 1.246 \pm 0.014$, $c = (1.35 \pm 0.67) \times 10^{-4}$ and $p = 1.065 \pm 0.001$. Confidence intervals here correspond to the range of values enclosing a 63% decrease of the likelihood function. Interestingly, these estimates of parameters A , α , c and p fall within the common range for seismicity observed in typical tectonic environments [Ogata, 1992]. This indicates that the self-triggering process in Ubaye is very similar to what is observed along major faults at plate boundaries [e.g., Helmstetter et al., 2003a; Marsan and Lengline, 2008]. We also interpret this close similarity as an indication that our modeling procedure properly succeeded at separating both contributions from, on one hand, the nonstationary forcing and on the other hand, the cascading process of secondary aftershocks.

[34] The resulting model (Figure 7, black curve) of the swarm seismicity rate is in very good agreement with the rate observed at JAUF (Figure 7, gray curve). Figure 7 also displays the contribution of the nonstationary forcing rate $\lambda_0(t)$ (dashed curve) to the total seismicity rate of the Ubaye swarm. The forcing-induced activity rate increases progressively from the beginning of the swarm up to its apex between day 174 (23 June 2003) and day 350 (16 December 2003), when it led to about 5 events per day. Afterward, this forcing slowly and progressively weakens toward the end of 2004. The general evolution of the forcing rate consequently presents an evolution that is quite similar to the overall trend of observed activity. This is an indication that low-frequency variations of the earthquake rate may be related to a slow and progressive external forcing mechanism, while high-frequency variations may be related to cascades of aftershocks sequences. We also note that our model fails at

reproducing the amplitude of the four prominent peaks of seismic activity occurring at days 174, 198, 243, and 276. This failure is a direct consequence of the definition of $\lambda_0(t)$ as a stair-step function. Indeed, by keeping a constant value for $\lambda_0(t)$ in each time window, we prevent the model to adapt rapid fluctuations of the background forcing rate, probably related with strong transients of the fluid overpressure.

[35] As explained in section 4.1, our estimates of the background rate rely on Hainzl et al.'s [2006] method. In Table 1 we also provide estimates obtained from two other procedures. The first alternative technique consists in inverting jointly the ETAS epidemic parameters and background values for all windows (we use time windows as presented in Figure 7). The second alternative technique attempted at reconstructing the background rate from the difference between the observed rate of event and the rate of triggered events (estimated from the ETAS triggering kernel using A , α , c and p estimates presented in this section). This daily background rate estimate was initially smoothed over a 100 day time window, and afterward averaged for each of the time windows defined above. Although the joint inversion technique delivers background rate values quite close to estimates using Hainzl et al.'s [2006] method, the second alternative "background reconstruction" technique show higher discrepancies in respect to this method. Such differences between background rate estimates for these two techniques (see Table 1) may partly be due to the smoothing used for the background reconstruction technique (alternative 2), and to the use of different sets of parameters A , α , c , and p . However, all of background rate estimation techniques explained here present overall a reasonable level of coherency, and background rate estimates undergo very similar evolution patterns.

[36] For the next part of the analysis, we use the background estimates obtained using the modified change-point procedure described in section 4.1. This technique presents the advantages of being the most objective, and the most appropriate method to decluster the Ubaye data set. Alternative modeling using time windows with constant duration, or constant number of events have proved to lead to worse adjustments, in terms of BIC values. Best results have been obtained using the modified change-point technique.

5. Retrieval of Effective Stress Changes

[37] In this section, we estimate changes in effective stress (normal stress minus pore pressure) using the earthquake rate at JAUF declustered from its epidemic cascades of aftershocks. The link between the seismicity rate and stress changes arises from the constitutive laws based on rate-and-state friction and proposed by Dieterich [1994].

[38] In the following, we hypothesize that the rate $\lambda_0(t)$ is directly related to a time-dependent change in effective stress within the swarm area. According to the Mohr-Coulomb criterion a decrease of the effective stress $\sigma = \sigma_n - \bar{p}$ may favor the friction of rocks (i.e., earthquake occurrence) by unclamping faults at depth. Such a decrease of the effective stress can either be related to a decrease in normal stress σ_n , or to an increase in pore pressure \bar{p} . This also amounts to consider that cascades of secondary aftershocks ($\lambda(t) - \lambda_0(t)$) reflect the amount of seismicity triggered by shear stress changes on optimally oriented fault planes.

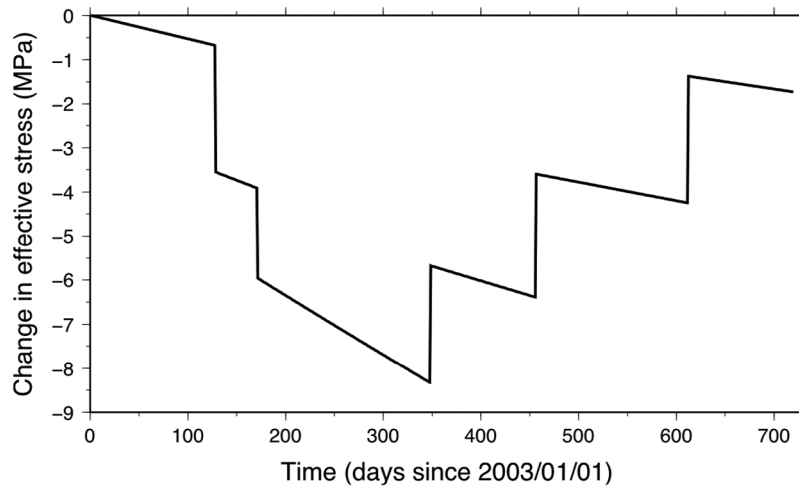


Figure 8. Changes in effective stress integrated over the swarm area. These changes are estimated from the rate of background event $\lambda_0(t)$ represented in Figure 7 and by use of rate-and-state constitutive laws for earthquake production [Dieterich, 1994; Dieterich et al., 2000] (see section 5). We supposed that this seismicity rate was triggered by changes in effective stress under a constant shear stressing rate of 2.5×10^{-3} MPa yr $^{-1}$. Effective stress is expressed relatively to the steady state value of 83.4 MPa before the swarm initiation. This value comes from the difference in overburden pressure (with bulk density $\rho = 2700$ kg m $^{-3}$) minus the hydrostatic pressure at $z = 5$ km.

[39] Dieterich et al. [2000] showed that local Coulomb stress changes could be estimated from the temporal changes of the seismicity rate in a given region. According to these authors, there is a nonlinear relationship between stress changes and seismicity rates for a population of faults governed by rate-and-state friction laws [Dieterich, 1994]. The seismicity rate R depends on a state variable γ according to

$$R = \frac{r}{\gamma \dot{\tau}_r} \quad (16)$$

where r is a reference seismicity rate under a reference shear stressing rate $\dot{\tau}_r$. The evolution of the state variable γ is governed by the following differential equation:

$$d\gamma = \frac{1}{A'\sigma} \left[dt - \gamma d\tau + \gamma \left(\frac{\tau}{\sigma} - k \right) d\sigma \right] \quad (17)$$

where A' and k are constitutive parameters, σ stands for effective stress, and τ stands for shear stress.

[40] Here, we set $R(t) = \lambda_0(t)$, and we calculate $\gamma(t)$ by use of equation (16). We use a quasi-static formulation of equation (17) with time steps of length $dt = 1$ day. For each time step, $\sigma(t + dt)$ corresponds to $\sigma(t) + d\sigma$, where $d\sigma$ is obtained by solving equation (17). In other words, we assume a constant stressing rate for shear stress ($d\tau = \dot{\tau} dt$) and a quasi-static evolution of effective stress $d\sigma$ and γ , with $d\gamma = \gamma(t + dt) - \gamma(t)$. This approach tends to underestimate large amplitude, short-lived changes in $|\delta\sigma|$ as the background rate is averaged over longer time intervals (see the discussion on time windows in section 4.1).

[41] We select parameters values according to values reported in the literature. We consider a secular linear increase in shear stress with time of $\dot{\tau} = 2.5$ kPa yr $^{-1}$ on the basis of geodetic estimates in the area [Ferhat et al., 1998] and on a shear modulus equal to 0.25×10^{11} Pa. This hypothesis for shear stress changes appeared as the most

reasonable owing to the likely influence of fluid pressure on the swarm activity. In addition, to the authors' knowledge, no complementary geodetic data set exists to better constrain the evolution of $d\tau$ during this episode. The reference earthquake rate r for $M_L \geq 0$ is estimated from the rate r_1 of $M_L \geq 1$ event located in the area between 1989 and 2002, when no prominent seismic activity occurred. We obtain $r_1 = 0.3$ event/yr with $M_L \geq 1$ from the relocated catalog, which leads to $r = r_1 \times 10^{b(1-0.2)} = 2.74$ events/yr with $M_L \geq 0.2$. We express changes in effective stress relatively to a reference steady state value σ_0 before the swarm initiation. We choose σ_0 to be equal to the overburden pressure (with bulk density $\rho = 2700$ kg m $^{-3}$) minus the hydrostatic pressure at 5 km depth. This leads to a steady state effective stress of $\sigma_0 = 83$ MPa. According to equation (17) the amplitude of effective stress changes $d\sigma$ is directly related to σ_0 . We have also observed that the relative height of stress steps increases when σ_0 increases. As a consequence, the selection of initial hydrostatic conditions thus represents a lower bound for changes in effective stress; that is, a higher bound for changes in pore pressure. Initial shear stress was chosen to be equal to 0.6 times the steady state effective stress; i.e., we suppose the crust to be close to a critical state for rupture. Laboratory measurements suggest that the A' parameter usually ranges between 0.005 and 0.015 [Dieterich et al., 2000]. As we have no a priori knowledge on pressure and temperature conditions within the source volume, we choose an average value; i.e., $A' = 0.01$. The resulting amplitude of effective stress is also related to the value of parameter A' (see equation (17)), although stress changes remain of the same order. That is, we obtained maximum stress changes of -3 and of -9 MPa for A' equal to 0.005 and 0.015, respectively. Parameter k is set equal to 0.23 [Linker and Dieterich, 1992].

[42] Figure 8 displays the effective stress history obtained using this procedure. The step-like shape is obviously

unrealistic but is directly inherited from assumptions on $\lambda_0(t)$. This curve should consequently be understood as a first-order estimate of effective stress changes during the swarm. Negative changes in effective stress mean that the triggering of microearthquakes during the Ubaye swarm occurred either by a decrease in normal stress or by an increase in pore fluid pressure. Finally, if one assumes constant normal stress conditions, this result suggests that a pore pressure increase of about 8 MPa was sufficient to generate 41% (1448 background events) of the seismic activity in Ubaye between January 2003 and December 2004.

6. Discussion

[43] In sections 3 and 4, we have shown that the Ubaye swarm (1) occurred on a simple planar structure striking N130°E and dipping 80°W, (2) exhibited an unusual diffusive migration of hypocenters toward the SE, and (3) required the contribution of an external nonstationary forcing rate in addition to the self-triggering of seismicity (via cascades of secondary aftershocks). Assuming that fluid circulations at depth induced a significant part of this activity, we explain the migration of earthquake hypocenters as the result of a fluid diffusion process within the crystalline basement. Moreover, the distribution of seismicity along a preferential plane suggests that fluids may have propagated through a more permeable channel, possibly inherited from a preexisting fault structure. The diffusive migration of hypocenters during the swarm is also an indication that fluid overpressure at depth was not high enough to open new fractures in the medium.

[44] The evocation of deep fluid circulation is of common use for explaining the spatial and temporal properties of seismic swarms [Horálek and Fischer, 2008]. In Ubaye, although no fluid outflow was observed during the sequence, we propose that a fluid overpressure at depth was responsible for the 2003–2004 swarm episode. First, this proposition relies on the similarity of the earthquake migration pattern with those observed during other swarm episodes that have been convincingly related with fluid circulations [Tsuneishi and Nakamura, 1970; Horálek and Fischer, 2008]. Second, it also relies on considerations about the present and past fluid circulations in the same bedrock, observed few kilometers further south. Recalling that the swarm activity was confined within a 3 to 8 km band at depth, the seismogenic structure of the swarm is most probably confined within the crystalline bedrock, rather than within the overlying 1 to 2 km thick Embrunais-Ubaye nappe [Jenatton *et al.*, 2007]. The bedrock crops out few kilometers south of the Ubaye valley, forming the Argentera Massif. In this massif, numerous outcropping fault structures and rock weathering related with fluid circulations can be studied directly in the field. Fault structures show preferential orientations along a direction subparallel to the swarm alignment [see Baietto *et al.*, 2009, and references therein]. Furthermore, several places in the Argentera Massif are well known for their geothermal activity, like Bagni di Vinadio, Italia, or Terme di Valdieri, Italia, about 15 km southeast of the former (Figure 1). Baietto *et al.* [2008, 2009]

studied the geological settings related with geothermal circulations in these areas. They reported an important fluid outflow at Terme di Valdieri, with a bulk discharge rate of 50 kg.s⁻¹ and a fluid temperature reaching up to 70°C. According to these authors, fluids chemical properties are also consistent with a circulation path within the crystalline basement, that is, going down to 5–6 km depth below the surface. As a consequence, the involvement of fluid circulations within the basement in Ubaye appears a very reasonable hypothesis, and is quite consistent with circulation depth estimated in the Argentera area.

[45] The analysis presented in section 5 shows that changes in effective stress can be estimated by use of the complete form of the differential equation for rate-and-state constitutive laws (see equation (17)). Assuming constant normal stress during the sequence, a progressive increase in pore pressure up to about 8 MPa could be sufficient to trigger the 16,147 events swarm. Figure 8 also shows that pore pressure progressively increased to this maximum value in 350 days, and decreased afterward by 7 MPa in about 350 days. This slow evolution of the pore pressure may explain the particularly long duration of this swarm episode.

[46] These estimates of pore pressure change are in good agreement with numerical modeling of fluid circulations during swarm episodes, and with observations from fluid injection experiments. In a recent study of the 1965–1967 Matsushiro swarm in Japan, Cappa *et al.* [2009] argued that pore pressure changes of 4 MPa were necessary to quantitatively reproduce the observed seismicity, deformation, and fluid outflow at the surface. Hainzl and Ogata [2005] also found that a pore fluid diffusion mechanism with a maximum pore pressure change of 2 to 5 MPa was compatible with the seismic properties of the Vogtland-West Bohemia swarm. In another example, Miller *et al.* [2004] showed that CO₂ pore pressure changes of about 10–20 MPa can explain the spatial migration of the 1997 sequence of 6 M > 5 earthquakes in central Italy. These authors also argued that such changes in pore pressure are large enough to overwhelm static shear stress changes. In Ubaye, we find that for pore pressure changes of about 8 MPa, shear stress transfers (leading to successive cascades of aftershocks) could still induce 59% of the seismic activity. Our estimates also agree with the results of Cornet *et al.* [1997], who reported seismicity in response to overpressure between 5 and 10 MPa during the 1993 fluid injection experiment at Soultz-sous-Forêts, France. The initiation of the swarm activity for very slight pore pressure changes (<1 MPa) during the first days of 2003 is also very consistent with the conclusions of Zoback and Harjes [1997] and Shapiro *et al.* [2006a] and confirms the critical state of the fault before the swarm episode.

[47] Toda and Stein [2002] proposed that earthquake swarms might be driven by change in shear stressing rate. They proposed that according to this principle, aftershock duration would decrease with increasing shear stressing rate changes. However, we show here that the decrease in effective stress due to pore pressure diffusion at depth constitutes another viable explanation for swarm generation. Our results also indicate that the seismicity in Ubaye area

results from the superposition of a time-varying external forcing over cascades of seismicity with constant aftershock duration.

7. Conclusion

[48] We have presented a new analysis of the Ubaye seismic swarm. This study relies on the catalog built by the French Sismalp seismological network, which we improved by relocating 974 earthquakes. We also used the time series of 16,147 event detections at station JAUF in 2003–2004. We have identified a clear spatial migration of earthquakes, along a subvertical N130°E fault structure. We interpreted this as the result of fluid circulation at depth. Thus, the initiation and development of the Ubaye swarm could be related to the diffusive propagation of fluid overpressure within the crystalline basement. An important result of this study is the assessment of the associated fluid overpressure from the analysis of the earthquake rate. This calculation is based on rate-and-state constitutive laws applied to the nonstationary rate of fluid-driven (i.e., background) seismicity. We found that pore fluid pressure varied with time during the swarm sequence, with a maximum excess of pore pressure of 8 MPa, with respect to the level that preexisted before January 2003. This value is comparable with estimates from numerical modeling of swarms in Italy and in Japan, or with direct pressure measurements realized during fluid injection experiments.

[49] Besides, some aspects of the fracture process still remain open questions, and could not be addressed within the framework of the present study. For example, was the permeable channel localized within the core or within the damage zone of the source fault? What was the physico-chemical nature of fluids involved? How can we model their path to the seismogenic zone? Did the presence of the overlying nappes in Ubaye played a role in the structure design of the source?

[50] Each of these aspects needs further investigation in the framework of a careful geological study of the area. Clarifying the process of fluid refill, its behavior at depth and its interplay with the basement geology are now essential steps to consider for a comprehensive explanation of episodic swarm occurrences in the Ubaye valley, and worldwide.

[51] **Acknowledgments.** E.P. was supported by the CNRS-ANR ASEISMIC project. We also acknowledge the following institutions for their support: Conseil Général de l'Isère, the Délégation aux Risques Majeurs (French Ministry of the Environment), the Institut National des Sciences de l'Univers (CNRS), and the Conseil Régional Rhône-Alpes funded the Sismalp network. The Bureau Central Sismologique Français, the regional direction of the Environment (Dreal Rhône-Alpes), the Observatoire de Grenoble (OSUG), and the Conseils Généraux (Isère, Alpes-de-Haute-Provence, Hautes-Alpes, Haute-Savoie, Ain, and Savoie) support its running costs. The authors would like to thank the Associate Editor and two anonymous referees for their thorough reviews and helpful suggestions.

References

- Aki, K., and P. G. Richards (2002), *Quantitative Seismology*, 2nd ed., 704 pp., Univ. Sci., Herndon, Va.
- Baietto, A., P. Cadoppi, G. Martinotti, P. Perello, P. Perrochet, and F.-D. Vuataz (2008), Assessment of thermal circulations in strike-slip fault systems: The Terme di Valdieri case (Italian western Alps), *Geol. Soc. Spec. Publ.*, 299, 317–339.
- Baietto, A., P. Perello, P. Cadoppi, and G. Martinotti (2009), Alpine tectonic evolution and thermal water circulations of the Argentera Massif (southwestern Alps), *Swiss J. Geosci.*, 102, 223–245, doi:10.1007/s00015-009-1313-5.
- Bräuer, K., H. Kämpf, and G. Strauch (2009), Earthquake swarms in non-volcanic regions: What fluids have to say, *Geophys. Res. Lett.*, 36, L17309, doi:10.1029/2009GL039615.
- Cappa, F., J. Rutqvist, and K. Yamamoto (2009), Modeling crustal deformation and rupture processes related to upwelling of deep CO₂-rich fluids during the 1965–1967 Matsushiro earthquake swarm in Japan, *J. Geophys. Res.*, 114, B10304, doi:10.1029/2009JB006398.
- Chiodini, G., F. Frondini, C. Cardellini, F. Parello, and L. Peruzzi (2000), Rate of diffuse carbon dioxide Earth degassing estimated from carbon balance of regional aquifers: The case central Apennine, Italy, *J. Geophys. Res.*, 105, 8423–8434, doi:10.1029/1999JB900355.
- Cornet, F. H., J. Helm, H. Poitrenaud, and A. Etchecopar (1997), Seismic and aseismic slips induced by large-scale fluid injections, *Pure Appl. Geophys.*, 150, 563–583, doi:10.1007/s000240050093.
- Davison, A. C. (2003), *Statistical Models*, 726 pp., Cambridge Univ. Press, New York.
- Dieterich, J. H. (1994), A constitutive law for rate of earthquake production and its application to earthquake clustering, *J. Geophys. Res.*, 99, 2601–2618, doi:10.1029/93JB02581.
- Dieterich, J. H., V. Cayol, and P. Okubo (2000), The use of earthquake rate changes as a stress meter at Kilauea volcano, *Nature*, 408, 457–460, doi:10.1038/35044054.
- Farrell, J., S. Husen, and R. B. Smith (2009), Earthquake swarm and *b*-value characterization of the Yellowstone volcano-tectonic system, *J. Volcanol. Geotherm. Res.*, 188, 260–276, doi:10.1016/j.jvolgeores.2009.08.008.
- Fehler, M., L. House, and H. Kaieda (1987), Determining planes along which earthquakes occur: Method and application to earthquakes accompanying hydraulic fracturing, *J. Geophys. Res.*, 92, 9407–9414, doi:10.1029/JB092iB09p09407.
- Ferhat, G., K. L. Feigl, J.-F. Ritz, and A. Souriau (1998), Geodetic measurement of tectonic deformation in the southern Alps and Provence, France, 1947–1994, *Earth Planet. Sci. Lett.*, 159, 35–46, doi:10.1016/S0012-821X(98)00065-X.
- Fréchet, J., and N. Pavoni (1979), Etude de la sismicité de la zone Briançonnaise entre Pelvoux et Argentera (Alpes Occidentales) à l'aide d'un réseau de stations portables, *Eclogae Geol. Helv.*, 72, 763–779.
- Gutenberg, B., and C. F. Richter (1956), Earthquake magnitude, intensity, energy, and acceleration, *Bull. Seismol. Soc. Am.*, 46, 105–145.
- Guyoton, F., J. Fréchet, and F. Thouvenot (1990), La crise sismique de janvier 1989 en Haute-Ubaye (Alpes de Haute Provence, France): Étude fine de la sismicité par le nouveau réseau SISMALP, *C. R. Acad. Sci., Ser. II*, 311, 985–991.
- Hainzl, S., and T. Kraft (2006), Analysis of complex seismicity pattern generated by fluid diffusion and aftershock triggering, paper presented at the 4th International Workshop on Statistical Seismology (STATSEI4), Inst. of Stat. Math., Kanagawa, Japan, 9–13 Jan.
- Hainzl, S., and Y. Ogata (2005), Detecting fluid signals in seismicity data through statistical earthquake modeling, *J. Geophys. Res.*, 110, B05S07, doi:10.1029/2004JB003247.
- Hainzl, S., F. Scherbaum, and C. Beauval (2006), Estimating background activity based on interevent-time distribution, *Bull. Seismol. Soc. Am.*, 96, 313–320, doi:10.1785/0120050053.
- Helmstetter, A., D. Sornette, and J.-R. Grasso (2003a), Mainshocks are aftershocks of conditional foreshocks: How do foreshock statistical properties emerge from aftershock laws, *J. Geophys. Res.*, 108(B1), 2046, doi:10.1029/2002JB001991.
- Helmstetter, A., G. Ouillon, and D. Sornette (2003b), Are aftershocks of large Californian earthquakes diffusing?, *J. Geophys. Res.*, 108(B10), 2483, doi:10.1029/2003JB002503.
- Hill, D. P. (1977), A model for earthquake swarm, *J. Geophys. Res.*, 82, 1347–1352, doi:10.1029/JB082i008p01347.
- Hill, D. P., and S. Prejean (2005), Magmatic unrest beneath Mammoth Mountain, California, *J. Volcanol. Geotherm. Res.*, 146, 257–283, doi:10.1016/j.jvolgeores.2005.03.002.
- Horálek, J., and T. Fischer (2008), Role of crustal fluids in triggering the West Bohemia/Vogtland earthquake swarms: Just what we know (a review), *Stud. Geophys. Geod.*, 52, 455–478, doi:10.1007/s11200-008-0032-0.
- Huc, M., and I. G. Main (2003), Anomalous stress diffusion in earthquake triggering: Correlation length, time dependence, and directionality, *J. Geophys. Res.*, 108(B7), 2324, doi:10.1029/2001JB001645.
- Janatton, L., R. Guiguet, F. Thouvenot, and N. Daix (2007), The 16,000-event 2003–2004 earthquake swarm in Ubaye (French Alps), *J. Geophys. Res.*, 112, B11304, doi:10.1029/2006JB004878.

- Kagan, Y. Y., and L. Knopoff (1987), Statistical short-term earthquake prediction, *Science*, *236*, 1563–1567, doi:10.1126/science.236.4808.1563.
- Linker, M. F., and J. H. Dieterich (1992), Effect of variable normal stress on rock friction: Observations and constitutive equations, *J. Geophys. Res.*, *97*, 4923–4940, doi:10.1029/92JB00017.
- Llenos, A. L., J. J. McGuire, and Y. Ogata (2009), Modeling seismic swarms triggered by aseismic transients, *Earth Planet. Sci. Lett.*, *281*, 59–69, doi:10.1016/j.epsl.2009.02.011.
- Lohman, R. B., and J. J. McGuire (2007), Earthquake swarms driven by aseismic creep in the Salton Trough, California, *J. Geophys. Res.*, *112*, B04405, doi:10.1029/2006JB004596.
- Marsan, D., and O. Lengline (2008), Extending earthquakes' reach through cascading, *Science*, *319*, 1076–1079, doi:10.1126/science.1148783.
- Marsan, D., C. J. Bean, S. Steacy, and J. McCloskey (1999), Spatio-temporal analysis of stress diffusion in a mining-induced seismicity system, *Geophys. Res. Lett.*, *26*, 3697–3700, doi:10.1029/1999GL010829.
- Marsan, D., C. J. Bean, S. Steacy, and J. McCloskey (2000), Observation of diffusion processes in earthquake populations and implications for the predictability of seismicity systems, *J. Geophys. Res.*, *105*, 28,081–28,094, doi:10.1029/2000JB900232.
- Matsu'ura, R. S., and I. Karakama (2005), A point-process analysis of the Matsushiro earthquake swarm sequence: The effect of water on earthquake occurrence, *Pure Appl. Geophys.*, *162*, 1319–1345, doi:10.1007/s00024-005-2672-0.
- Miller, S. A., C. Colletini, L. Chiaraluce, M. Cocco, M. Barchi, and B. J. P. Kaus (2004), Aftershocks driven by a high-pressure CO₂ source at depth, *Nature*, *427*, 724–727, doi:10.1038/nature02251.
- Noir, J., E. Jacques, S. Békri, P. M. Adler, P. Tapponnier, and G. C. P. King (1997), Fluid flow triggered migration of events in the 1989 Dobi earthquake sequence of Central Afar, *Geophys. Res. Lett.*, *24*, 2335–2338, doi:10.1029/97GL02182.
- Nur, A., and J. R. Booker (1972), Aftershocks caused by pore fluid flow?, *Science*, *175*, 885–887, doi:10.1126/science.175.4024.885.
- Ogata, Y. (1988), Statistical models for earthquake occurrences and residual analysis for point processes, *J. Am. Stat. Assoc.*, *83*, 9–27, doi:10.2307/2288914.
- Ogata, Y. (1992), Detection of precursory relative quiescence before great earthquakes through a statistical model, *J. Geophys. Res.*, *97*, 19,845–19,871, doi:10.1029/92JB00708.
- Savage, J. C., and R. S. Cockerham (1984), Earthquake swarm in Long Valley Caldera, California, January 1983: Evidence for dike inflation, *J. Geophys. Res.*, *89*, 8315–8324, doi:10.1029/JB089iB10p08315.
- Shapiro, S. A., and C. Dinske (2009), Scaling of seismicity induced by non-linear fluid-rock interaction, *J. Geophys. Res.*, *114*, B09307, doi:10.1029/2008JB006145.
- Shapiro, S. A., E. Huenges, and G. Borm (1997), Estimating the crust permeability from fluid-injection-induced seismic emission at the KTB site, *Geophys. J. Int.*, *131*, F15–F18, doi:10.1111/j.1365-246X.1997.tb01215.x.
- Shapiro, S. A., J. Kummerow, C. Dinske, G. Asch, E. Rothert, J. Erzinger, H.-J. Kämpel, and R. Kind (2006a), Fluid induced seismicity guided by a continental fault: Injection experiment of 2004/2005 at the German Deep Drilling Site (KTB), *Geophys. Res. Lett.*, *33*, L01309, doi:10.1029/2005GL024659.
- Shapiro, S. A., C. Dinske, and E. Rothert (2006b), Hydraulic-fracturing controlled dynamics of microseismic clouds, *Geophys. Res. Lett.*, *33*, L14312, doi:10.1029/2006GL026365.
- Sue, C. (1998), Dynamique actuelle et récente des Alpes occidentales internes—Approches structurales et sismologique, Ph.D. thesis, Univ. Joseph Fourier, Grenoble, France.
- Thouvenot, F., and J. Fréchet (2006), Seismicity along the northwestern edge of the Adria microplate, in *The Adria Microplate: GPS Geodesy, Tectonics, and Hazards*, edited by N. Pinter et al., pp. 335–349, Springer, Dordrecht, Netherlands, doi:10.1007/1-4020-4235-3_23.
- Thouvenot, F., J. Fréchet, F. Guyot, R. Guiguet, and L. Jenatton (1990), Sismalp: An automatic phone-interrogated seismic network for the western Alps, *Cah. Cent. Eur. Geodyn. Sismol.*, *1*, 1–10.
- Toda, S., and R. Stein (2002), Evidence for the AD 2000 Izu islands earthquake swarm that stressing rate governs seismicity, *Nature*, *419*, 58–61, doi:10.1038/nature00997.
- Tsuneishi, Y., and K. Nakamura (1970), Faulting associated with the Matsushiro swarm earthquakes, *Bull. Earthquake Res. Inst. Univ. Tokyo*, *48*, 29–51.
- Ukawa, M., and H. Tsukahara (1996), Earthquake swarms and dike intrusions off the east coast of Izu Peninsula, central Japan, *Tectonophysics*, *253*, 285–303, doi:10.1016/0040-1951(95)00077-1.
- Waldhauser, F., and W. L. Ellsworth (2000), A double-difference earthquake location algorithm: Method and application to the Northern Hayward Fault, California, *Bull. Seismol. Soc. Am.*, *90*, 1353–1368, doi:10.1785/0120000006.
- Weinlich, F. H., K. Bräuer, H. Kämpf, G. Strauch, J. Tesär, and S. M. Weise (1999), An active subcontinental mantle volatile system in the Western Eger rift, central Europe: Gas flux, isotopic (He, C, and N) and compositional fingerprints, *Geochim. Cosmochim. Acta*, *63*, 3653–3671, doi:10.1016/S0016-7037(99)00187-8.
- Yamashita, T. (1999), Pore creation due to fault slip in a fluid-permeated fault zone and its effect on seismicity: Generation mechanism of earthquake swarm, *Pure Appl. Geophys.*, *155*, 625–647, doi:10.1007/s000240050280.
- Zoback, M. D., and H.-P. Harjes (1997), Injection-induced earthquakes and crustal stress at 9 km depth at the KTB deep drilling site, Germany, *J. Geophys. Res.*, *102*, 18,477–18,491, doi:10.1029/96JB02814.

G. Daniel, UMR 6249 Chrono Environnement, Université de Franche-Comté, CNRS, 16 route de Gray, F-25030 Besançon, France. (guillaume.daniel@univ-fcomte.fr)

J. L. Got, D. Marsan, and E. Prono, LGIT, Université de Savoie, CNRS, Observatoire de Grenoble, F-73376 Le Bourget du Lac, France.

R. Guiguet, A. Helmstetter, L. Jenatton, F. Thouvenot, and P. Traversa, LGCA, Université Joseph Fourier-Grenoble I, CNRS, Observatoire de Grenoble, BP 53, F-38041 Grenoble, France.

S. Hainzl, Institute of Geosciences, University of Potsdam, POB 60 15 53, D-14415, Potsdam, Germany.

F. Renard, Physics of Geological Processes, University of Oslo, PO Box 1048 Blindern, N-0316 Oslo, Norway.